Molecular Biology of the Cell
Vol. 11, 325–337, January 2000

Identification of Filamin as a Novel Ligand for Caveolin-1: Evidence for the Organization of Caveolin-1–associated Membrane Domains by the Actin Cytoskeleton

Martin Stahlhut and Bo van Deurs*

Structural Cell Biology Unit, Department of Medical Anatomy, The Panum Institute, University of Copenhagen, DK-2200 Copenhagen N, Denmark

Submitted June 1, 1999; Revised October 12, 1999; Accepted November 9, 1999
Monitoring Editor: Guido Guidotti

Reports on the ultrastructure of cells as well as biochemical data have, for several years, been indicating a connection between caveolae and the actin cytoskeleton. Here, using a yeast two-hybrid approach, we have identified the F-actin cross-linking protein filamin as a ligand for the caveolae-associated protein caveolin-1. Binding of caveolin-1 to filamin involved the N-terminal region of caveolin-1 and the C terminus of filamin close to the filamin-dimerization domain. In in vitro binding assays, recombinant caveolin-1 bound to both nonmuscle and muscle filamin, indicating that the interaction might not be cell type specific. With the use of confocal microscopy, colocalization of caveolin-1 and filamin was observed in elongated patches at the plasma membrane. Remarkably, when stress fiber formation was induced with Rho-stimulating *Escherichia coli* cytotoxic necrotizing factor 1, the caveolin-1–positive structures became coaligned with stress fibers, indicating that there was a physical link connecting them. Immunogold double-labeling electron microscopy confirmed that caveolin-1–labeled racemose caveolae clusters were positive for filamin. The actin network, therefore, seems to be directly involved in the spatial organization of caveolin-1–associated membrane domains.

INTRODUCTION

Caveolins are an evolutionarily conserved family of 16- to 25-kDa cholesterol-binding integral membrane proteins functionally implicated in caveolae biogenesis, endocytic events, cholesterol transport, and various signal transduction processes (Parton, 1996; Anderson, 1998; Okamoto *et al.*, 1998). The best characterized member of the family, caveolin-1, a 21- to 24-kDa protein, was independently cloned as the main protein of the caveolar coat (Glenney and Soppet, 1992) and as the *trans*-Golgi network–derived vesicle-associated protein VIP21 (Kurzchalia *et al.*, 1992). Caveolin-1 is a marker protein for caveolae, 50- to 80-nm Ω-shaped plasma membrane invaginations, and can be found on the *trans*-Golgi network and vesicles as well. Caveolae represent cholesterol- and sphingolipid-rich membrane domains (Schroeder *et al.*, 1991; Rothberg *et al.*, 1992; Mukherjee *et al.*, 1998). Caveolin-1 and the related caveolin-2 are associated with morphologically identifiable caveolae, which in polarized epithelial cells are formed at the basolateral, but not the apical, membrane (Scherer *et al.*, 1997; Scheiffele *et al.*, 1998; Vogel *et al.*, 1998).

Attempts to isolate caveolar membrane fractions with the use of different methods have achieved ambiguous results with regard to protein composition (Sargiacomo *et al.*, 1993, 1995; Chang *et al.*, 1994; Schnitzer *et al.*, 1995; Smart *et al.*, 1995; Stan *et al.*, 1997). A major problem is verifying that no other sphingolipid-rich membrane domains contaminate the genuine caveolar fraction. The seemingly most promising report at this time uses an immunoisolation procedure for endothelial caveolae (Oh and Schnitzer, 1999). Proteins that can be copurified with caveolae comprise caveolin-1 and -2, annexin II, and several known caveolin-1 ligands: G-proteins (Li *et al.*, 1995), src family kinases (Li *et al.*, 1996), eNOS (Garcia-Cardena *et al.*, 1996), and PKCα (Oka *et al.*, 1997). A stretch of 20 amino acids in the N-terminal part of caveolin-1 (amino acids 82–101) seems to be responsible for a large part of these caveolin–protein ligand interactions and has been termed the "caveolin scaffolding domain" (Li *et al.*, 1996). Furthermore, screenings of phage display libraries with the caveolin-1 scaffolding domain have revealed a general caveolin-1–binding consensus sequence ($\phi X\phi XXXX\phi XX\phi$,

* Corresponding author. E-mail address: b.v.deurs@mai.ku.dk.

where ϕ indicates a hydrophobic amino acid and X indicates any amino acid) (Couet *et al.*, 1997).

Caveolin-1 expression is highest in white adipose and lung tissue and can be detected in other tissues as well as in many cell lines (Glenney, 1989; Scherer *et al.*, 1996, 1997). Upon oncogenic transformation, caveolin-1 is down-regulated in fibroblasts, and heterologous expression of caveolin-1 in transformed fibroblasts leads to abrogation of anchorage-independent growth (Koleske *et al.*, 1995; Engelman *et al.*, 1997). Caveolin-1 and caveolae are also down-regulated in response to angiogenic growth factors in vascular endothelial cells, an effect that can be counteracted by angiogenic inhibitors (Liu *et al.*, 1999).

Two alternatively translated isoforms, caveolin-1α and caveolin-1β, distinguished by the lack of 31 N-terminal amino acids in the latter, have been detected (Scherer *et al.*, 1995). Both isoforms have the ability to oligomerize into high-molecular-weight complexes of 14 or more monomers, resulting in molecular masses of up to 600 kDa (Monier *et al.*, 1995; Sargiacomo *et al.*, 1995). Furthermore, hetero-oligomers containing caveolin-1 and -2 can be formed (Scherer *et al.*, 1997). Because of an unusual hairpin-like membrane domain, both the N and C termini of caveolin-1 are exposed to the cytoplasm (Dupree *et al.*, 1993).

Ultrastructural and biochemical analyses have implicated the actin cytoskeleton in caveolae function (Rohlich and Allison, 1976; van Deurs *et al.*, 1982; Petersen *et al.*, 1989; Parton *et al.*, 1994; Fujimoto *et al.*, 1995). However, the molecular basis for binding of caveolae to the actin cytoskeleton has not been established. Here, using a yeast two-hybrid screen, we have identified the actin-binding protein filamin as a novel ligand for caveolin-1. The two-hybrid interaction could be validated by in vitro binding assays, and partial colocalization of filamin and caveolin-1 could be detected with the use of confocal microscopy and immunoelectron microscopy. Furthermore, caveolin-1 was present in filamin-positive patches at the plasma membrane, and it became dramatically coaligned with actin stress fibers upon Rho stimulation.

MATERIALS AND METHODS

Construction of Plasmids

pVIP21 encoding canine caveolin-1 (courtesy of Dr. K. Simons, EMBL, Heidelberg, Germany) served as a template for the PCR amplification of four caveolin cDNA fragments with the use of Pfu polymerase (Stratagene, La Jolla, CA). The primer pair CTAGGATCCGCATGTCTGGGGGCAAATACG (MS501)/CTCCTCCTCGAGTCAGCGGTAAAACCAGTA (MS307) was used for caveolin-1-1–303 (encoding amino acids 1–101), CTAGGATCCCCATGGCGGAGGAGATGAGC (MS502)/MS307 was used for caveolin-1-94–303 (encoding amino acids 32–101), MS501/CTCCTCCTCGAGCTAGGTTTCTTTCTGC (MS304) was used for caveolin-1-1–534 (encoding amino acids 1–178), and MS502/MS304 was used for caveolin-1-94–534 (encoding amino acids 32–178) cDNA amplification. The fragments were cut with *Bam*HI/*Xho*I and subcloned into the *Bam*HI/*Xho*I sites of pACT-2 (Clontech, Palo Alto, CA). The resulting plasmids were designated pTc1-1–303, pTc1-94–303, pTc1-1–534, and pTc1-94–534, respectively. They encoded Gal4-activation domain (Gal4-AD)–caveolin-1 hybrid proteins. Caveolin-1-1–303 and caveolin-1-94–303 fragments were cut with *Bam*HI/*Xho*I from the plasmids pTc1-1–303 and pTc1-94–303, respectively, and subcloned into the *Bam*HI/*Sal*I sites of pAS2-1 (Clontech). This resulted in the plasmids pSc1-1–303 and pSc1-94–303, respectively, encoding Gal4 DNA–binding domain (Gal4-BD)–caveolin-1 hybrid proteins. pSc1-1–303 was used as the bait in a yeast two-hybrid screen. The plasmid pTfilamin-28 was obtained from the two-hybrid screening (see below).

GST–canine caveolin-1 fusion protein expression vectors were constructed by subcloning *Bam*HI/*Xho*I caveolin-1 cDNA fragments derived from the pTc1 plasmids into the *Bam*HI/*Sal*I sites of pGEX-5X-2 (Amersham Pharmacia Biotech, Uppsala, Sweden). Histidine-tagged expression vectors were constructed with the use of the pQE series (Qiagen, Hilden, Germany). pQE32-filamin-28 was made by subcloning the 1260-base pair *Bam*HI/*Xho*I fragment from pTfilamin-28 into the *Bam*HI/*Sal*I sites of pQE32 (Qiagen). The histidine tag, containing six consecutive histidine residues, was at the N terminus of the filamin fragments.

Expression vectors encoding the caveolin-2 N terminus or subfragments of the filamin-28 fragment were made by subcloning the appropriate PCR-amplified or restriction fragments into the plasmids with the use of standard techniques. The correctness of the ORFs was confirmed in all cases by sequencing with the Thermo-Sequenase system (Amersham Pharmacia Biotech).

Yeast Two-Hybrid Techniques

Strains Y187(a) and Y190(α), supplied by the Matchmaker 2 two-hybrid system (Clontech), were grown in complete or appropriate minimal synthetic dropout (SD) medium. Y187 was used only for the mating control assay to verify true two-hybrid interactions. All transformations followed a high-efficiency transformation protocol (Gietz and Schiestl, 1995).

Transformants were grown for 3–7 d at 30°C on either minimal medium agar lacking Trp and Leu (SD/−W/−L) or minimal medium agar lacking His, Trp, and Leu and containing 25 mM 3-aminotriazole (SD/−H/−W/−L/25) to suppress residual histidine synthesis in the strain Y190.

For colony-lift filter assays of lacZ reporter gene expression, yeasts were grown on SD/−W/−L agar. After freezing and thawing of replica filters, they were incubated with 0.3 mg/ml X-gal (Advanced Biotechnologies, Surrey, England) in 100 mM sodium phosphate, pH 7.0, 10 mM KCl, 1 mM $MgSO_4$, and 0.27% (vol/vol) β-mercaptoethanol for several hours.

Quantitative determinations of β-galactosidase activities were performed on Y190 cells grown in SD/−W/−L with the use of *o*-nitrophenyl-galactopyranoside (Sigma-Aldrich, St. Louis, MO) as the substrate, according to the instructions in the Matchmaker 2 manual.

Purification of GST and His$_6$ Fusion Proteins

Overnight cultures of the *Escherichia coli* strain BL21 carrying the appropriate GST expression vector were diluted 1:10 into prewarmed Luria-Bertani medium containing 100 μg/ml ampicillin (Pierce, Rockford, IL) and incubated at 37°C until the OD_{600} was between 0.7 and 0.9. Expression of the GST fusion proteins was subsequently induced with 1 mM isopropyl-thio-galactopyranoside (Amersham Pharmacia Biotech). Cells were harvested after 3 h (GST), 2 h (GST–caveolin-1-1–101 and GST–caveolin-1-32–178), or 1 h (GST–caveolin-1-1–178). Cell pellets were frozen at −20°C. Fusion proteins were batch purified with the use of lysozyme and *N*-lauroylsarkosine as described (Frangioni and Neel, 1993). In brief, bacteria were thawed on ice and incubated in STE buffer (150 mM NaCl, 10 mM Tris-HCl, 1 mM EDTA, pH 8.0) containing 100 μg/ml lysozyme. *N*-Lauroylsarkosins was added to a final concentration of 1.5% (wt/vol) to lyse the cells. After addition of DTT to 5 mM, cells were sonicated briefly with a microprobe (IKA, Staufen, Germany). Debris and insoluble proteins were pelleted at 15,000 × *g*, and the supernatant was adjusted to 2% (vol/vol) Triton X-100.

To the supernatant, glutathione–Sepharose (Amersham Pharmacia Biotech) was added and incubated at room temperature for 30 min. The resin was rinsed five times with STE buffer and stored at 4°C.

Histidine-tagged proteins were expressed in the F′ episome-carrying bacterial strain M15 with the use of 29 μg/ml kanamycin (Merck, Darmstadt, Germany) and 100 μg/ml ampicillin. A protocol similar to that used for GST fusion proteins was used. However, lysozyme was used at 1 mg/ml, and detergents, DTT, and EDTA were omitted from the buffers. Ni-NTA–agarose (Qiagen) was used as the affinity matrix. Bound protein was rinsed five times with 50 mM sodium phosphate, 300 mM NaCl, 10% (vol/vol) glycerol, pH 6.0, and His_6–filamin-28 eluted with 500 mM imidazole in PBS, pH 7.2.

Protein concentrations were determined with the use of the D_C assay (Bio-Rad, Hercules, CA).

Binding Assays

Sixty micrograms of GST or GST–caveolin-1-1–101 prebound to glutathione–Sepharose was incubated with 60 μg of His_6–filamin-28 in 500 μl of PBS, pH 7.2, at room temperature for 1 h. The resin was sequentially rinsed with PBS/0.1% Triton X-100 and PBS/0.5% Triton X-100, and bound proteins were dissolved in SDS-PAGE sample buffer.

Purified chicken muscle filamin (1.8 μg; Sigma-Aldrich) was incubated with 5 μg of the appropriate GST fusion protein (GST alone, GST–caveolin-1-1–101, GST–caveolin-1-1–178, or GST–caveolin-1-32–178) in 100 μl of STE/1% Triton X-100 for 2 h at 4°C. The resin was rinsed three times with 1 ml of STE/1% Triton X-100, and bound proteins were dissolved in sample buffer.

Antibodies

The polyclonal anti-caveolin-1 antibody (pac) was from Transduction Laboratories (Lexington, KY) and was diluted 1:10,000 for Western blotting and 1:200 for immunohistochemistry. The monoclonal anti-filamin antibody mab1680 (diluted 1:20–1:40 for immunohistochemistry), donkey serum, and double-labeling-certified fluorescein-conjugated donkey anti-mouse and rhodamine-conjugated donkey anti-rabbit antibodies were from Chemicon (Temecula, CA). The fluorescent antibodies were diluted 1:50.

A polyclonal antiserum against chicken filamin was from Sigma-Aldrich and was diluted 1:1500. The anti-GST antibody was from a GST-detection kit (Boehringer Mannheim/Roche, Hvidovre, Denmark) and was diluted 1:1000. The anti-penta-histidine antibody was from Qiagen and was diluted 1:2000. Peroxidase-coupled swine anti-rabbit and rabbit anti-goat secondary antibodies were from DAKO (Roskilde, Denmark). The peroxidase-coupled donkey anti-mouse antibody was from Amersham Pharmacia Biotech. These antibodies were diluted according to the recommendations of the manufacturers.

Because the tested commercially available anti-filamin antibodies did not recognize mouse filamin, a polyclonal antiserum against the histidine-tagged mouse filamin fragment isolated in the two-hybrid screen was raised in rabbits (pab228). The antiserum was diluted 1:3000 for Western blotting and 1:500 for immunohistochemistry.

SDS-PAGE and Western Blotting

Proteins were separated on 4–20% Tris-glycine precast gels (Novex, San Diego, CA). Proteins were electrotransferred onto Hybond P membranes (Amersham Pharmacia Biotech). Unspecific binding sites were blocked in 5% skim milk (Bio-Rad, Copenhagen, Denmark) in Dulbecco's PBS/0.05% Tween-20 (MPBST). The primary antibody was applied for 1 h at room temperature in MPBST, followed by three rinses with Dulbecco's PBS/0.05% Tween-20 (PBST). The peroxidase-coupled secondary antibody was then applied for 1 h at room temperature in MPBST followed by three rinses with PBST. Immunoreactivity was detected with the use of the ECL reagent and ECL hyperfilm (Amersham Pharmacia Biotech). Histidine-tagged proteins were detected in a similar way with the use of 1% casein in Tris-buffered saline, pH 7.5, instead of MPBST. The washing buffer contained 0.05% Tween-20, 0.2% Triton X-100, and 350 mM NaCl in Tris-buffered saline.

Immunodetection of GST fusion proteins was performed according to the manual with the use of components of the GST-detection kit (Boehringer Mannheim/Roche), with the exception of the chemiluminescence substrate, for which ECL was used.

Cell Culture

NIH/3T3 fibroblasts (obtained from the Fibiger Institute, Copenhagen, Denmark) and the SV40-immortalized trophoblast cell line T4.5 (courtesy of Dr. Ulla Wewer, Institute of Molecular Pathology, Copenhagen, Denmark) were cultured in DMEM containing 10% (vol/vol) FBS (Life Technologies, Albertslund, Denmark), penicillin, and streptomycin. T4.5 cells also received 50 μg/ml G418 (Life Technologies). Media and antibiotics except for G418 were obtained from the Department of Microbiology, Panum Institute (Copenhagen, Denmark). Cytotoxic necrotizing factor 1 (CNF-1; kindly provided by Dr. P. Boquet, Nice, France) was used at a concentration of 1×10^{-10} M for the indicated times. Cytochalasin D (CD) (Sigma-Aldrich) was used at 10 μg/ml for 15 min.

Immunofluorescence and Confocal Microscopy

NIH/3T3 cells or T4.5 cells grown on fibronectin-coated glass slides (Becton-Dickinson, Meylan, France) or glass coverslips were rinsed with PBS and fixed with 2% formaldehyde in PBS, pH 7.2, for 15 min. Cells were rinsed twice with PBS and permeabilized with 0.1% Triton X-100 in PBS for 10 min. Cells were rinsed once with PBS, and unspecific binding was blocked with 5% donkey serum in PBS for 30 min. Primary antibodies were incubated in 5% donkey serum in PBS for 60 min at room temperature. Cells were rinsed three times for 10 min with PBS and incubated with the secondary antibodies for 30 min in 5% donkey serum in PBS. Cells were rinsed four times for 10 min, all fluid was removed, and samples were mounted with the use of Fluoromount-G antibleaching medium (Southern Biotechnology Associates, Birmingham, AL). Samples were viewed and evaluated with the use of an LSM510 confocal microscope (Zeiss, Jena, Germany) with 40× or 63× Zeiss C-Apochromat water immersion objectives (numerical aperture 1.2). For rhodamine, a 543-nm He–Ne laser combined with a 560-nm long-pass filter was used, and for fluorescein, a 488-nm Ar laser combined with a 505-nm long-pass filter or a 505- to 530-nm band-pass filter (dual-channel recordings) was used.

Electron Microscopy

T4.5 trophoblasts were grown to semiconfluence on 60-mm Petri dishes (Nunc, Roskilde, Denmark) and treated with CNF-1 for 24 h. Cells were fixed in 25 mM HEPES, pH 7.2, 150 mM NaCl, 3 mM picric acid, 3% formaldehyde (Smart *et al.*, 1994). Cells were scraped from the dishes, sedimented at room temperature for 30 min, and pelleted for 1 min at 8000 rpm in an Eppendorf centrifuge. The pellet was rinsed with PBS and embedded in 7.5% gelatin (Oetker, Bielefeld, Germany) in PBS for 30 min at 37°C. After cooling on ice and trimming, cell pellets were infused first with 2.1 M sucrose for 30 min and then with 2.3 M sucrose for 30 min. Specimens were then mounted on aluminum stubs and frozen in liquid nitrogen. Eighty-nanometer sections were cut with the use of a Reichert Ultracut S microtome (Leica, Glostrup, Denmark), collected in 2.3 M sucrose, and mounted on Formvar-coated copper grids. Grids were incubated with pac (1:50) followed by protein A conjugated to 10-nm gold (purchased from Dr. G. Posthuma, Department of Cell Biology, Medical School, Utrecht, The Netherlands), and subsequently with mab1680 (1:20) followed by anti-mouse immunoglobulins conjugated to 5-nm gold (Amersham Pharmacia Biotech), according to a standard method (Slot *et al.*, 1991). After contrasting with uranyl acetate, sections were analyzed in an electron microscope (model 100 CM, Philips, Eindhoven, The Netherlands).

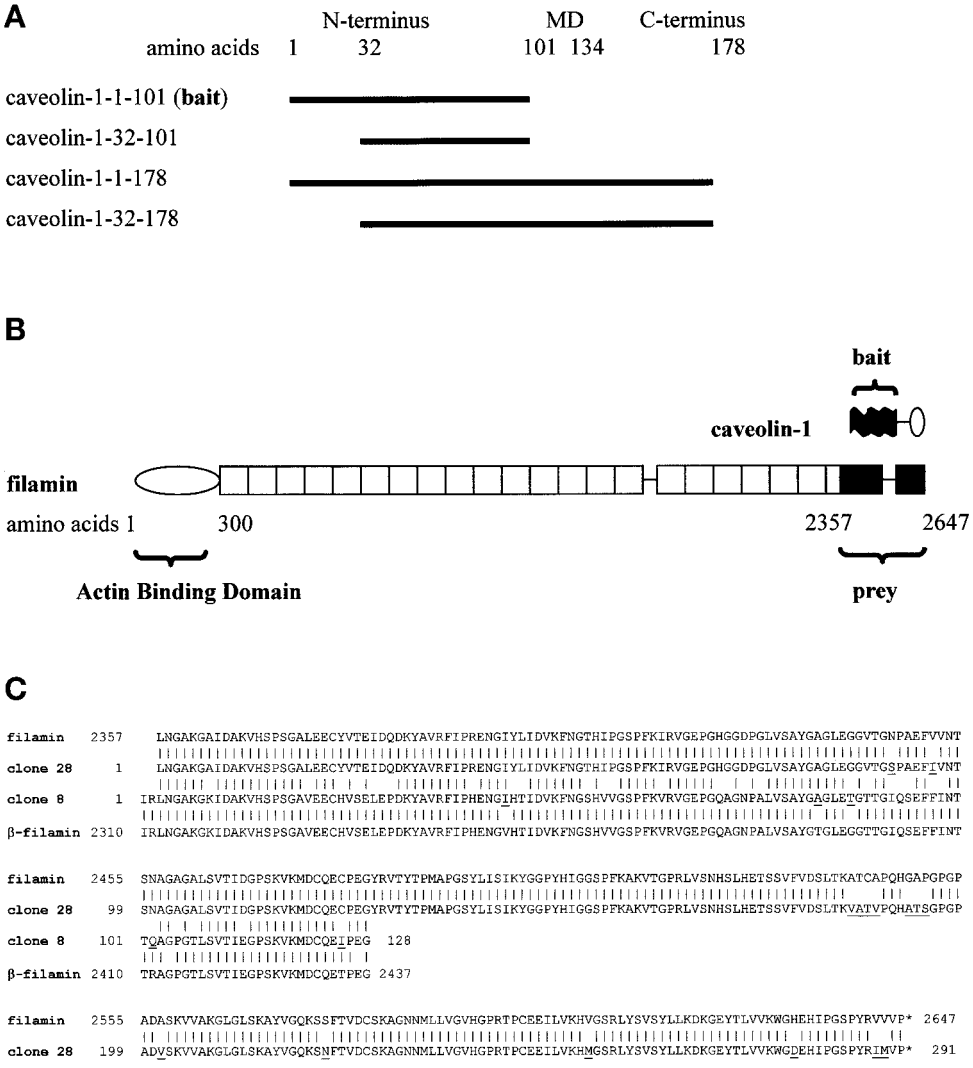

Figure 1. (A) Domain organization of caveolin-1. Amino acids 1–101 represent the N-terminal domain, amino acids 102–134 represent the membrane domain (MD), and amino acids 135–178 represent the C-terminal domain. Two variants of the N-terminal domain (caveolin-1-1–101 and caveolin-1-32–101) and the full-length proteins caveolin-1α (caveolin-1-1–178) and caveolin-1β (caveolin-1-32–178) were analyzed. Caveolin-1-1–101 was used as the bait in the two-hybrid screen. (B) Domain organization of filamin and comparison of the sizes of caveolin-1 and filamin. (Top) The N terminus (black) of caveolin-1α was used as the bait in the two-hybrid screen. The membrane domain and the C-terminal domain of caveolin-1 are indicated by a line and an oval, respectively. (Bottom) The rod-like filamin molecule has an N-terminal actin-binding domain followed by 24 homologous repeats of 96 amino acids each. The fragment of filamin obtained in the two-hybrid screen (prey) is shown in black. Two hinges are present at the connections between repeats 15–16 and 23–24. (C) Alignment of the amino acid sequences of the human filamin and β-filamin isoforms and the two amino acid sequences of the filamin fragments isolated in the two-hybrid screening. Over the sequenced region, human filamin (GenBank accession number P21333) and human β-filamin (GenBank accession number AF042166) are 95 and 96% identical to clones 28 and 8, respectively. Clone 28 is 76% identical to clone 8. The high homologies clearly identified clones 28 and 8 as fragments of mouse filamin and β-filamin, respectively. Species-specific differences in the amino acid sequences in the two-hybrid clones are underlined.

RESULTS

Identification of Two Filamin Isoforms as Ligands for Caveolin-1 in a Two-Hybrid Screen

The unusual hairpin-like topology of caveolins exposes both their N and C termini to the cytosol. The caveolin-1 membrane domain is believed to span amino acids 102–134 (Kurzchalia *et al.*, 1992). We chose the N-terminal 101 amino acids of caveolin-1 (caveolin-1-1–101; Figure 1A) as the "bait" for a two-hybrid screening, because (a) this part of the protein is involved in certain protein–protein interactions (shown for the caveolin scaffolding domain [amino acids 82–101]), and (b) it is not subject to lipid modifications, as is the C terminus, which could prevent hybrid protein translocation into the yeast nucleus necessary for reporter gene activation. The caveolin-1-1–101-Gal4-BD hybrid protein (apparent molecular weight, 38,000) could be detected in pSc1-1–303-transformed yeast cell lysates by an anti-caveolin-1 antibody. A commercial cDNA expression library, constructed in pACT2 from mRNA derived from NIH/3T3 cells, was the source of the "prey." A total of 1.2×10^6 clones was screened after cotransformation of the Y190 yeast strain with pSc1-1–303 and the NIH/3T3 cDNA library.

Fourteen truly positive clones were identified. Sequencing of the Gal4-AD plasmids revealed that five of the cDNAs coded for fragments of the constitutively expressed heat-shock protein Hsp84, three showed homology to nuclear helicases, one encoded a lim domain, another encoded a J domain of a murine DnaJ homologue, a third represented an ORF present in GenBank with no homology to known proteins, and two were short ORFs with unclear significance. The coding region of one clone (clone 28) was fully sequenced and found to represent nonmuscle filamin (ABP280, α-filamin), hereafter called filamin (Figure 1B) (Gorlin *et al.*, 1990). Sequencing of the first 350 bases of the coding region of another clone (clone 8) allowed unequivo-

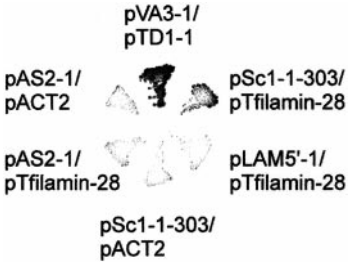

Figure 2. Growth of Y190 clones on SD/−H/−W/−L minimal medium containing 25 mM 3-aminotriazole. Yeast strain Y190 was transformed with the indicated combinations of plasmids. Only yeast cells coexpressing caveolin-1-1–101 and filamin-28 (pSc1-1–303/pTfilamin-28) and p53 and large T-antigen hybrid proteins (pVA3-1/pTD1-1; positive control), but not clones cotransformed with negative control combinations of plasmids, grew on this stringent selection medium, indicating true two-hybrid interactions.

cal identification of the protein product as β-filamin (Takafuta *et al.*, 1998). These two cDNAs coded for amino acids 2357–2647 of filamin and amino acids 2310–2602 of β-filamin, respectively. Sequence alignments showed that the first amino acid in clone 28 corresponded to the third amino acid in clone 8 (Figure 1C). Thus, the two clones represented nearly identical regions of the homologous filamins.

The isolated cDNAs encoded the very C-terminal regions of the ~280-kDa rod-like proteins. Filamins form homodimers and contain an N-terminal actin-binding domain that is followed by 24 repeats each of 96 amino acids. Repeat 24 is required for filamin dimerization. Thus, the isolated fragments were at a long distance from the actin-binding site and included the dimerization domain.

Filamin seems to be highly conserved among species, because the translations of the mouse cDNA sequences were 95% identical to the published human sequences. The similarity of clone 28 to clone 8 was somewhat less (75% identity), corresponding well to the overall identity of human filamin to human β-filamin (70%).

Y190 double transformed with pSc1-1–303 and pTfilamin-28 grew on minimal agar lacking histidine, tryptophan, and leucine in the presence of 25 mM 3-aminotriazole, an inhibitor of histidine biosynthesis required to suppress leakiness of the histidine deficiency in strain Y190 (Figure 2). Y190 double transformed with negative control combinations of plasmids did not grow on this medium. These controls comprised the combinations pAS2-1 (Gal4-BD alone)/pACT2 (Gal4-AD alone), pAS2-1/pTfilamin-28, pSc1-1–303 (caveolin-1-1–101)/pACT2, and pLAM5′-1 (human lamin C_{66-230})/pTfilamin-28. The established interaction between the murine p53 C terminus and the SV40 T-antigen with the use of the plasmid combination pVA3-1/pTD1-1 served as a positive control.

Quantification of the Two-Hybrid Interaction of Caveolin-1 with Filamin

With the use of a colony-lift filter assay, Trp^+Leu^+ Y190 colonies expressing caveolin-1 and filamin fragments stained blue with X-gal. To obtain information about the strength of the caveolin-1–filamin interaction, β-galactosidase reporter gene activities of various Y190 double transformants were measured with the use of a fluid-phase enzyme assay (Figure 3). Binding affinities between caveolin-1 and filamin were significantly greater than those of the negative controls ($p < 0.005$; two-tailed *t* test for samples with unequal variances). The caveolin-1-1–101-filamin-28 interaction produced 2.3 mU of β-galactosidase activity, and the caveolin-1-32–101-filamin-28 interaction produced 3.8 mU of β-galactosidase activity, whereas negative controls scored <0.55 mU. Apparently, the N-terminal 31 amino acids of caveolin-1 were not necessary for the filamin–caveolin-1 interaction. Moreover, caveolin-1-32–101 scored consistently greater reporter gene activities than caveolin-1-1–101 in the interaction with filamin. Statistical analysis of the data, with the one-tailed *t* test for samples with unequal variances, indicated that the affinities of caveolin-1-1–101 and caveolin-1-32–101 for filamin were significantly different ($p = 0.037$). Also, the nonparametric Mann-Whitney U test estimated a significant difference between the binding data for caveolin-1-1–101 and caveolin-1-32–101 fragments ($U < 0.05$). These quantifications indicated that the 31 N-terminal amino acids of caveolin-1 might be able to negatively modulate the caveolin-1–filamin interaction.

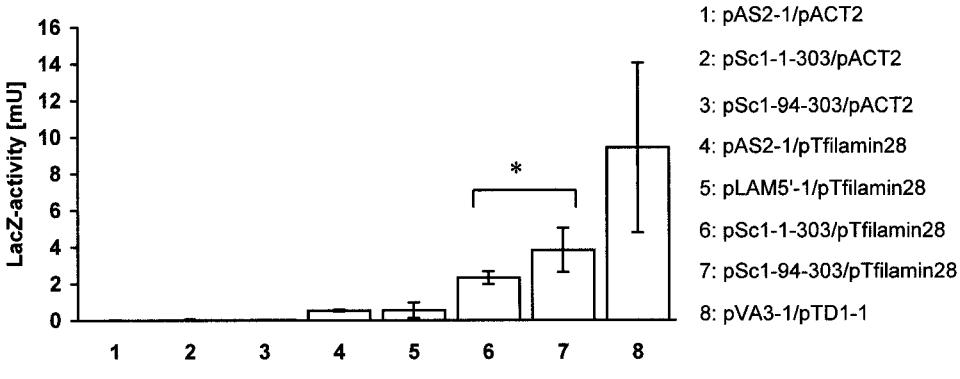

Figure 3. Quantitative analysis of the binding strength between caveolin-1 and filamin hybrid proteins. Double-transformed yeast strain Y190 was grown in minimal medium lacking tryptophan and leucine and lysed, and β-galactosidase reporter gene activity was measured in a fluid-phase assay. The binding strengths of the two caveolin-1 hybrid proteins to the filamin-28 hybrid protein (6 and 7) were significantly greater ($p < 0.005$) than the binding strengths of the control interactions (1–5) and corresponded to approximately one-third of the strength of the interaction between p53 and T-antigen hybrid proteins (8). The interaction of caveolin-1-1–101 with the filamin hybrid protein was significantly weaker than the caveolin-1-32–101-filamin interaction (*$p = 0.037$; one-tailed *t* test for samples with unequal variances). The data show the averaged means of four independent experiments performed in triplicate for each plasmid combination. Bars show SEM ($n = 4$).

Table 1. Interaction of caveolin-1 and caveolin-2 N termini with various fragments of filamin in two-hybrid experiments

Filamin repeats	Caveolin-1 (aa 1–101)	Caveolin-1 (aa 32–101)	Caveolin-2 (aa 1–86)
22-23-hinge-24 (aa 2357–2647)	+++	++++	−
22-23-hinge (aa 2357–2649)	++	+++	−
24 (aa 2550–2647)	−	−	−
23 (aa 2421–2516)	−	−	−
22 (aa 2357–2490)	−	−	−

aa, amino acids.

The established interaction of the p53 C terminus with the SV40 T-antigen produced 9.4 mU of β-galactosidase activity. Only the caveolin-1-1–101-filamin-28 interaction, but not the caveolin-1-32–101-filamin-28 interaction, was judged significantly lower than this positive control ($p < 0.05$).

Next, we mapped the caveolin-1–binding site in filamin by constructing expression vectors encoding smaller filamin fragments. We also included the N terminus of caveolin-2 in the analysis to determine if binding was specific for the caveolin-1 isoform. Table 1 summarizes the results. Apart from the originally isolated fragment, only a fragment containing filamin repeats 22 and 23 and the hinge region, but not repeats 22, 23, or 24 alone, was able to bind to caveolin-1. Again, binding to caveolin-1-32–101 was stronger than binding to caveolin-1-1–101. Caveolin-2-1–86 did not bind any of the filamin fragments. However, caveolin-2-1–86 bound to caveolin-1-32–101, and in another control experiment, filamin repeat 24 was shown to have dimerization capacity, indicating the functionality of these constructs (our unpublished results).

Thus, filamin interacted specifically with caveolin-1, but not with caveolin-2, and the interaction involved a region within repeats 22 and 23 and the hinge of filamin.

Visualization of β-galactosidase activity by probing caveolin-1 interactions with β-filamin (clone 8) took more time than visualization with clone 28, implying a weaker interaction with caveolin-1. Therefore, clone 28 was selected for further investigation.

Characterization of Fusion Proteins and a New Anti-Filamin Antiserum

To confirm the two-hybrid interaction with a different binding assay, three different GST–caveolin-1 fusion proteins (GST–caveolin-1-1–101, GST–caveolin-1-1–178, and GST–caveolin-1-32–178) and a hexa-histidine–tagged variant of the filamin-28 fragment (His_6–filamin-28) were constructed.

Figure 4A shows a Western blot detecting the four GST fusion proteins. GST alone migrated as a single band at 26 kDa. GST–caveolin-1-1–101 was present as a major band at 38 kDa, corresponding well to the calculated 11-kDa increase in molecular mass caused by the fused caveolin-1 fragment. GST–caveolin-1-1–178 migrated close to the expected 49 kDa, whereas GST–caveolin-1-32–178 migrated at 48 kDa. A few degradation products, mainly around 26 kDa, were also detectable in all GST–caveolin fusion protein preparations. A polyclonal anti-caveolin antibody recognized all three GST–caveolin-1 fusion proteins, but not GST alone (Figure 4B).

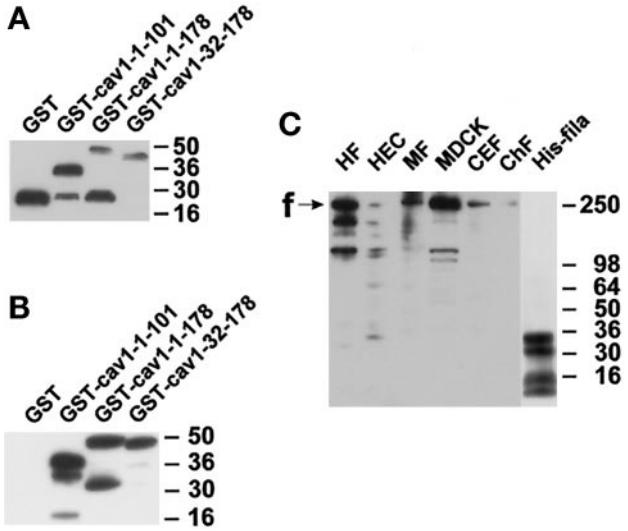

Figure 4. Characterization of fusion proteins and antibodies. Samples were separated by SDS-PAGE and electrotransferred onto polyvinylidene difluoride membranes. (A) Detection of GST fusion proteins with the use of an anti-GST antibody. GST appears as a single band at 26 kDa, whereas full-length and several degradation products are seen with GST–caveolin-1 fusion proteins. (B) Detection of the same GST fusion proteins as in A with the use of a polyclonal anti-caveolin-1 antibody. GST is not recognized. In contrast, the caveolin-1–containing proteins show strong immunoreactivity. (C) Specificity and cross-reactivity of the antiserum pab228. In cell lysates from human fibroblasts (HF), human endothelial cells (HEC), mouse 3T3-RSV fibroblasts (MF), Madin-Darby canine kidney cells (MDCK), and chicken embryonic fibroblasts (CEF), bands around 250 kDa and some smaller bands probably representing degradation products of filamin are recognized. Purified chicken filamin (ChF; 13 ng) is also recognized. The position of full-length filamin is indicated with "f." Four bands in the hexa-histidine–tagged filamin-28 isolate are detected (His-fila). The two upper bands probably reflect full-length and C-terminally shortened His_6–filamin-28 protein. Apparent molecular weights are indicated to the right in each panel.

It turned out that most commercially available antibodies to filamin did not recognize the His_6–filamin-28 protein. Therefore, we raised an antiserum, pab228, in a rabbit with the use of the purified His_6–filamin-28 protein as the immunogen. pab228 recognized a dominant band of ~250 kDa in human, murine, canine, and chicken cell lines. Furthermore, purified chicken muscle filamin was detected (Figure 4C). The size of the recognized proteins, as well as the recognition of nanogram amounts of purified chicken muscle filamin, were good indications that the antiserum recognized filamin from four different species. The lower bands probably represented calpain-mediated degradation products of filamin (Gorlin *et al.*, 1990). pab228 also seemed to be useful for immunocytochemistry (see below).

Four major bands were detected in bacteria expressing His_6–filamin-28, the largest one migrating at 35 kDa, close to the expected 34 kDa for His_6–filamin-28 (Figure 4C, His-fila). The second largest band (31 kDa) should represent a C-

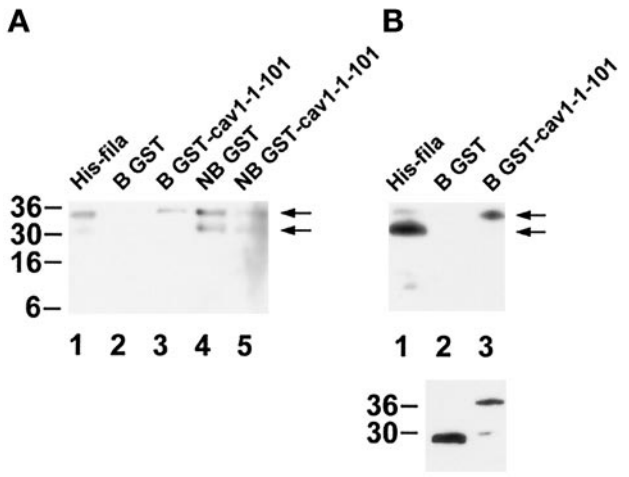

Figure 5. In vitro binding assay of GST–caveolin-1-1–101 to His_6–filamin-28. Samples were separated by SDS-PAGE and electrotransferred onto polyvinylidene difluoride membranes. (A) Immunodetection of His_6–filamin-28 with the use of the anti-penta-His antibody. The histidine tag is recognized in proteins of 35 and 31 kDa in the original His_6–filamin-28 fraction. No immunoreactivity is observed in the fraction bound to GST. The fraction bound to GST–caveolin-1-1–101 retains the full-length His_6–filamin-28 protein of 35 kDa, but not the C-terminally shortened protein of 31 kDa. Nonbound fractions contain both His_6–filamin-28 fragments (arrows). (B, upper panel) A pattern similar to that in A is observed with the use of the filamin-specific antiserum pab228. Four His_6–filamin-28 fragments are detected in the starting material (His-fila). Only the 35-kDa fragment is retained by GST–caveolin-1-1–101, whereas no His_6–filamin-28 protein is detected in the eluate containing GST. (B, lower panel) Detection of GST and GST–caveolin-1-1–101 in each eluate with the use of the anti-GST antibody. Apparent molecular weights are indicated to the left, and arrows designate the positions of full-length His_6–filamin-28 and a C-terminally shortened fragment in A and B.

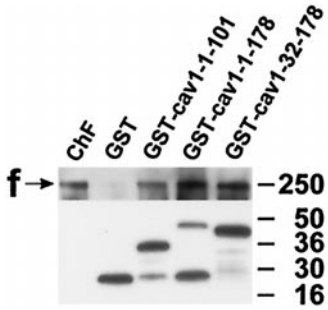

Figure 6. In vitro binding of GST–caveolin-1 fusion proteins to chicken muscle filamin. Samples were separated by SDS-PAGE and electrotransferred onto polyvinylidene difluoride membranes. (Upper panel) A chicken filamin-specific polyclonal antiserum recognizes filamin immunoreactivity of purified chicken muscle filamin (ChF) and in fractions containing GST–caveolin-1-1–101, GST–caveolin-1-1–178, and GST–caveolin-1-32–178. In the control eluate containing GST, only weak, residual binding is detected. (Lower panel) Immunoblot of the GST fusion proteins present in the eluates with the use of an anti-GST mAb. These results extend the data of filamin-28–caveolin-1 binding, showing that full-length caveolin-1 isoforms are able to bind to a muscle filamin isoform. Apparent molecular weights are indicated to the right. f, filamin.

terminally shortened fragment of His_6–filamin-28, because it was detected by an anti-penta-His antibody as well (Figure 5A). The nature of the smaller 10- to 14-kDa fragments was not investigated.

Binding of Caveolin-1 to Filamin In Vitro

To probe the specificity of the caveolin-1-1–101 fragment for the binding to filamin in vitro, GST or GST–caveolin-1-1–101, prebound to glutathione–Sepharose, was incubated with His_6–filamin-28, and the retained proteins were separated by SDS-PAGE. An anti-penta-His antibody detected a single band of 35 kDa in the GST–caveolin-1-1–101 (Figure 5A, lane 3) but not in the GST control sample (Figure 5A, lane 2). Interestingly, the 31-kDa band of His_6–filamin-28 was observed only in the nonbound fractions (Figure 5A, lanes 4 and 5). This was in contrast to the result from our two-hybrid experiments showing that the caveolin-1 N terminus was able to interact with a filamin fragment lacking repeat 24. Thus, in vitro, the integrity of filamin repeat 24 seemed to be important for caveolin-1 binding.

Probing the fractions with pab228 confirmed the result obtained with the anti-penta-His antibody. In the fraction of proteins bound to GST–caveolin-1-1–101, only the 35-kDa band, but not the 31-kDa band, of His_6–filamin-28 was detected (Figure 5B, upper panel). The lower panel of Figure 5B shows that approximately equal amounts of GST and GST–caveolin-1-1–101 were present in the eluates.

For the interaction between caveolin-1 and filamin to have any biological significance, it would be important to test not only protein fragments, but also the full-length proteins, for the capability to bind to each other. Because of the uncertainty regarding whether full-length caveolin-1 would work in the two-hybrid system and negative results from the oligomerization of full-length caveolin-1 with this system, GST fusion proteins containing caveolin-1-1–101, caveolin-1-1–178, or caveolin-1-32–178 were tested in a second binding assay. Purified chicken gizzard filamin was incubated with the GST fusion proteins under physiological salt conditions. Chicken gizzard filamin was easily detectable in the protein fractions bound to GST–caveolin-1-1–101, GST–caveolin-1-1–178, and GST–caveolin-1-32–178, but not when incubated with GST alone (Figure 6).

Thus, two in vitro binding assays confirmed the two-hybrid interaction between filamin and the N terminus of caveolin-1. Moreover, not only did filamin bind to the N-terminal domain of caveolin-1, it also bound to full-length caveolin-1α and -1β. Interestingly, both nonmuscle and muscle filamin were able to bind to caveolin-1, suggesting that the interaction might not be restricted to nonmuscle cells.

Immunolocalization of Caveolin-1 and Filamin

Confocal microscopy was used to localize filamin and caveolin-1. The antiserum pab228 and mab1680 were used to detect filamin in mouse NIH/3T3 fibroblasts and human T4.5 trophoblasts. Filamin immunoreactivity was dominant along stress fibers and in the cell periphery (Figure 7, A and

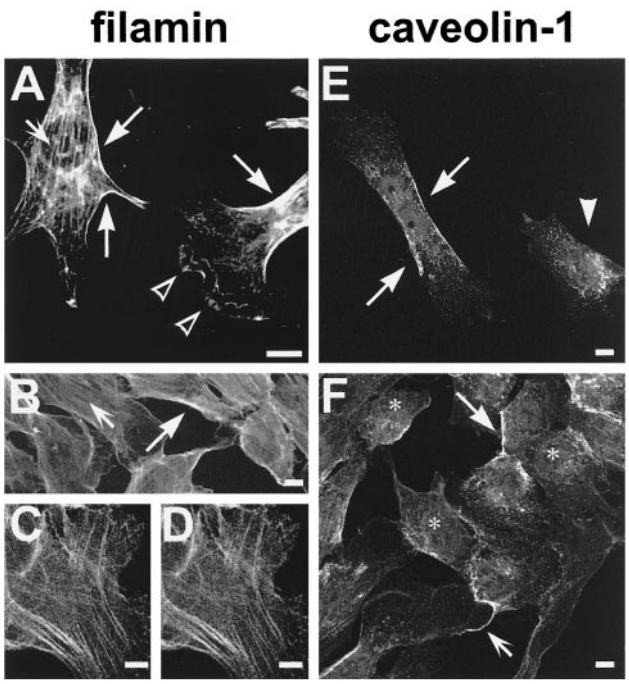

Figure 7. Confocal images of NIH/3T3 fibroblasts (A) and T4.5 trophoblasts (B–F) stained for filamin (A–D) or caveolin-1 (E and F). Filamin immunoreactivity was dominant on stress fibers (A and B, small arrows) and at the cell periphery (A and B, large arrows). Blurry immunoreactivity was seen in lamellipodia (A, open arrowheads). The labeling produced by antibodies mab1680 and pab228 is identical (compare C and D). Caveolin-1 was detected in patches or in a punctate pattern at the plasma membrane (E and F, large arrows) and along cellular processes (F, small arrow). The arrowhead in E designates a cell apparently showing only intracellular caveolin-1 immunoreactivity. Antibodies used were pab228 (A and C), mab1680 (B and D), and polyclonal anti-caveolin-1 (E and F). Bars, 10 μm.

B, arrows). Filamin staining in lamellipodia was patchy and somewhat blurry compared with the strong, string-like immunoreactivity underlying other membrane regions (Figure 7A, open arrowheads). Some diffuse cytoplasmic staining was also observed. The monoclonal anti-filamin antibody mab1680 and our polyclonal anti-filamin antiserum pab228 labeled the same structures in T4.5 cells, confirming the specificity of the antiserum (Figure 7, compare C and D).

In T4.5 trophoblasts, caveolin-1 was concentrated at the plasma membrane in elongated patches (Figure 7, E and F, large arrows). In addition, some caveolin-1 appeared to be intracellular, probably in a region reflecting the *trans*-Golgi network (Figure 7F, asterisks). Some cellular processes were also labeled for caveolin-1 (Figure 7F, small arrow). In a subpopulation of cells, virtually all caveolin-1 immunoreactivity was apparently cytoplasmic and no caveolin-1–positive patches at the membranes were observed (Figure 7E, arrowhead). The polyclonal anti-caveolin-1 antibody and the mAb 2234, raised against the 31 N-terminal amino acids of caveolin-1, produced highly similar staining patterns (Figure 7, compare E and F).

The observations in these immunolocalization experiments were in accordance with earlier reports on the localization of filamin and caveolin in various cell types (Dupree *et al.*, 1993; Provance *et al.*, 1993).

To determine if the filamin-positive regions of the plasma membrane also contained caveolin-1, trophoblasts were double labeled for these two proteins (Figure 8). Indeed, in many cases, the peripheral patchy or punctuate caveolin-1 structures appeared to be very close to the filamin-positive actin cables underlying the plasma membrane (Figure 8, A and B, arrows). A similar situation was seen in caveolin-1–positive cellular processes (Figure 8, C and D, arrowheads). Higher magnification showed coalignment of caveolin-1–positive patches with cortical filaments decorated with filamin (Figure 8A, detail, arrowheads). Larger patches lay between these filaments and apparently contacted them at their peripheries (Figure 8A, detail, arrow). These observations indicated that a part of the caveolin-1–positive plasma membrane domains, probably reflecting clusters of caveolae, could associate with filamin-decorated fibers.

It should be noted that there were generally only one or two major caveolin-1–positive patches per cell. Thus, a large part of the filamin-positive submembrane regions or processes were devoid of caveolin-1. Likewise, most intracellular caveolin-1 appeared to be spatially separated from filamin-positive filaments.

Rho Activation Reorganizes Caveolin-1-positive Membranes

Stress fibers are under the control of the small GTPase Rho (Ridley and Hall, 1992). The bacterial toxin CNF-1 constitutively activates Rho by deamidating glutamine 63, leading to increased stress fiber formation (Aktories, 1997). T4.5 trophoblasts grown on fibronectin in normal growth medium possessed some stress fibers and showed small, nonpolarized intracellular membrane domains of caveolin-1 (Figure 9A). After CNF-1 stimulation, large caveolin-1 patches were seen not only in the cellular cortex but also in patches following the orientation of certain stress fibers (Figure 9, B and C, arrowheads). These caveolin-1–positive assemblies along stress fibers were very large at the 3-h time point. After 24 h, the patches had developed into more numerous and generally slimmer assemblies than after 3 h (Figure 9, compare B and C). Furthermore, the amount of caveolin-1 seemed to increase. In the cell periphery, filamin and caveolin-1 were still found together in elongated patches in the presence of CNF-1 (Figure 9, A–C, large arrows). Treatment of the CNF-1–stimulated cells with CD disrupted stress fibers, and cell morphology changed rapidly to a spiky phenotype (Figure 9D). At the same time, the polarized, patchy cytoplasmic distribution of caveolin-1 was completely abolished, and only small, dispersed patches could be observed (Figure 9D, small arrows).

Thus, caveolin-1–positive membrane domains were remarkably reorganized after Rho activation, leading to a coalignment of these domains with filamin-decorated stress fibers. This organization could be abolished with CD. These observations strongly implied that caveolin-1–positive structures were physically linked to the actin filament system via filamin.

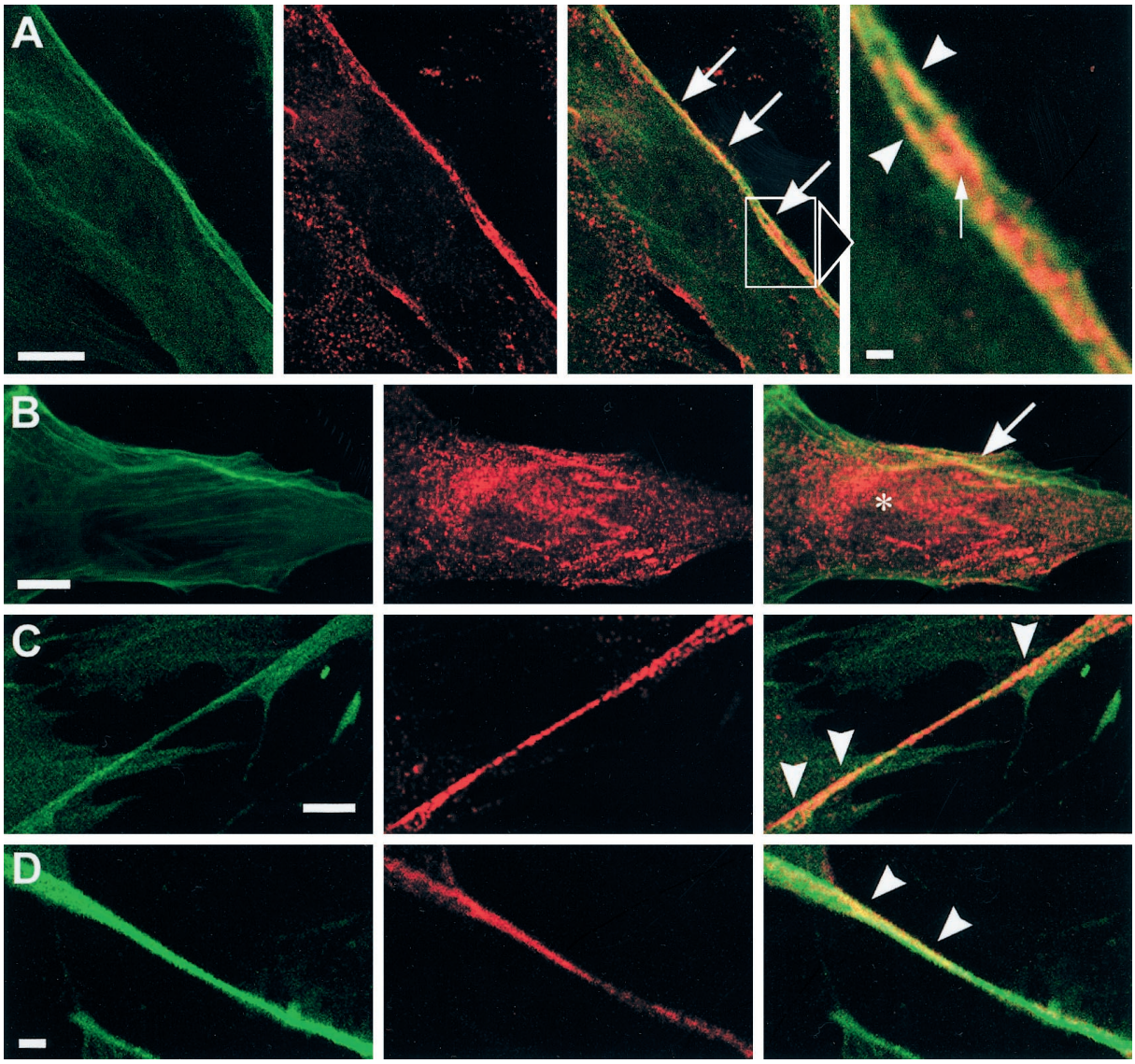

Figure 8. Confocal images of T4.5 trophoblasts double labeled for filamin and caveolin-1. (Left panels) Anti-filamin; (middle panels) anti-caveolin-1; (right panels) merged channels. (A and B) Filamin and caveolin-1 colocalize in patches at the cell periphery (large arrows). In addition, some caveolin-1 labeling appears to be intracellular (asterisk in B). The enlarged field in A shows a region of distinct coalignment of filamin and caveolin-1–positive structures at the plasma membrane. Caveolin-1 is present on (arrowheads) and between (small arrow) two filamin-positive fibers. (C and D) Codistribution of caveolin-1 and filamin in patches on cellular processes (arrowheads). Antibodies used were mab1680/polyclonal anti-caveolin-1 (A–C) and pab228/mab2234 (D). Bars, 10 μm (A–C), 1 μm (detail of A), and 5 μm (D).

Colocalization of Filamin with Clusters of Caveolae by Immunoelectron Microscopy

Because the optical resolution obtainable by confocal microscopy is two to three times the size of caveolae, it could not be determined whether the caveolin-1–positive membranes close to filamin-decorated filaments were single caveolae, groups of caveolae, or other kinds of immunoreactive structures. Therefore, we prepared ultracryosections of CNF-1–treated trophoblasts and double labeled them with antibodies against filamin and caveolin-1. The anti-caveolin-1 antibody specifically labeled plasma membrane caveolar invaginations. Generally, single caveolin-1–labeled caveolae were rare at the plasma membrane. Instead, they formed clusters of various sizes, often appearing as large racemose aggregates of caveolae (Figure 10). These were often deeply invaginated into the cell without losing surface contact (Figure 10B). Filamin labeling was sometimes seen very close to caveolae and the caveolar clusters at the cell surface. In contrast, filamin labeling was never found associated with clathrin-coated pits.

Thus, filamin seemed to colocalize with a fraction of clustered caveolae at the plasma membrane, an observation that fits well with the confocal microscopy data. Our findings thus

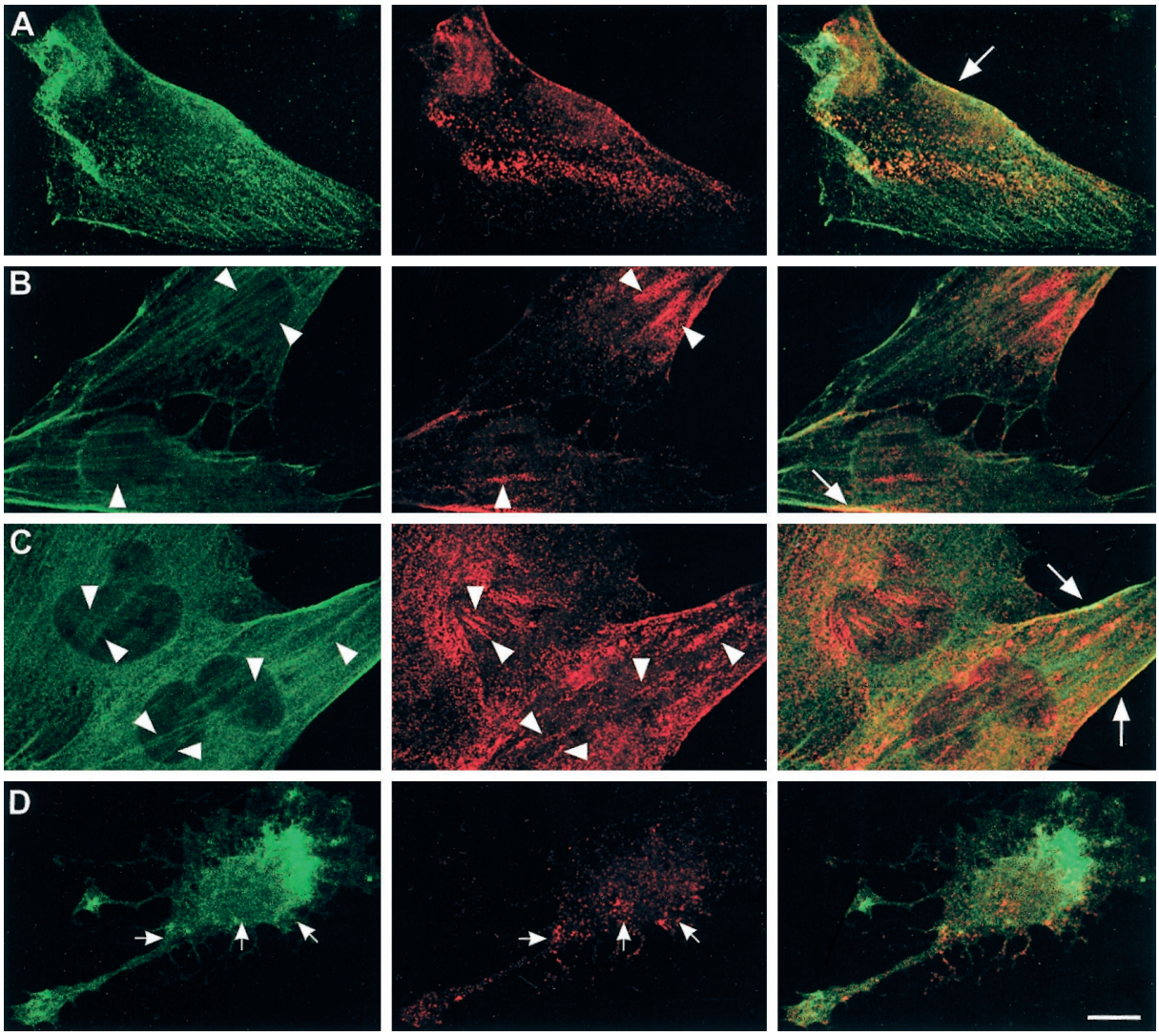

Figure 9. Reorganization of caveolin-1–positive structures in response to CNF-1 in T4.5 trophoblasts. (Left panels) anti-filamin; (middle panels) anti-caveolin-1; (right panels) merged channels. Compared with control conditions (A), 3 h after incubation with CNF-1 cells possessed very large clusters of caveolar membranes (B). These clusters became slimmer and more numerous after 24 h (C). In addition, more stress fibers were observed at both time points (B and C, left panels). Arrowheads in B and C indicate corresponding positions in the images showing filamin and caveolin-1, respectively, where caveolin-1 clusters coalign with stress fibers. Patches of caveolin-1 colocalized with filamin at the plasma membrane, as observed in control cells (A and Figure 8), could still be seen after treatment with CNF-1 (A–C, large arrows). Treatment of the cells with CD after a 3-h incubation with CNF-1 abolished stress fibers and the polarized distribution of caveolin-1 in the cytoplasm (D, small arrows). Bar, 10 μm.

provide strong evidence for the existence of an association of caveolin-1 and filamin not only in vitro but also in intact cells.

DISCUSSION

We have for the first time identified a cytoskeleton-associated protein, the actin cross-linking protein filamin, as a ligand for caveolin-1. With the use of a yeast two-hybrid screen, fragments of two isoforms of filamin, nonmuscle filamin and β-filamin, were isolated. Both fragments spanned about 300 amino acids of the filamin C terminus. These comprised the second half of filamin repeat 22, repeat 23, a hinge region, and the dimerization domain in repeat 24. Mapping of the filamin–caveolin-1 interaction in two-hybrid experiments revealed that the dimerization domain alone did not bind to caveolin-1. In contrast, the fragment spanning repeats 22 and 23 and the hinge was still able to bind to caveolin-1. Therefore, it seems likely that dimerization of filamin is not required for caveolin-1 binding. Because neither filamin repeat 22 or 23 alone bound to caveolin-1, the hinge region between repeat 23 and 24 seems to be a good candidate for the caveolin-1 binding site. Quantification of

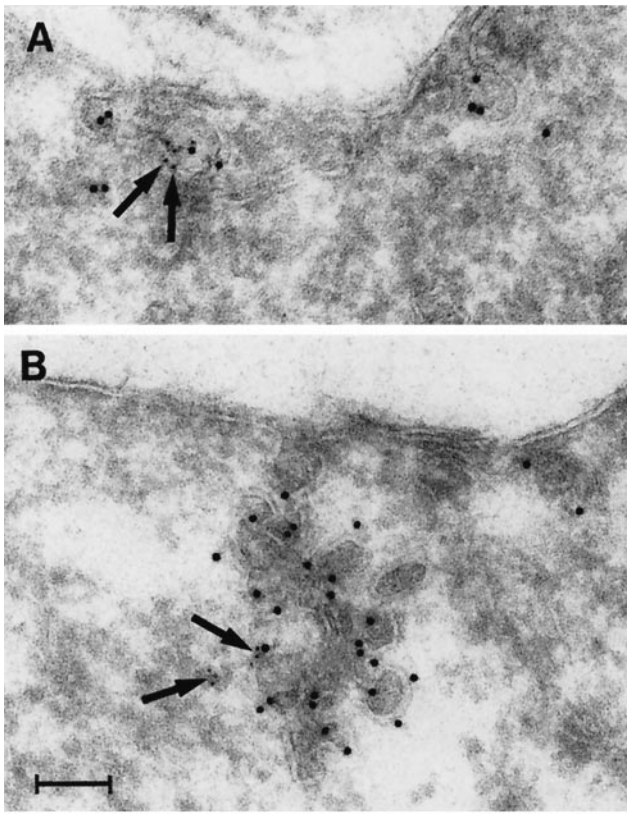

Figure 10. Localization of caveolin-1 and filamin in CNF-1–stimulated (24 h) T4.5 trophoblasts with the use of immunoelectron microscopy. (A) A small cluster of two caveolae is positive for caveolin-1 (10-nm gold). Filamin (5-nm gold; arrows) is present at the caveolar membrane. (B) Large racemose cluster of caveolae labeled for caveolin-1 (10-nm gold) and filamin (5-nm gold; arrows). The caveolae cluster invaginates deeply into the cell but is still surface connected. Bar, 100 nm.

the two-hybrid interaction revealed that the short N terminus of caveolin-1β (amino acids 32–101) was able to bind more strongly to filamin than the N terminus of caveolin-1α (amino acids 1–101), indicating a possible modulating influence of the 31 N-terminal amino acids on the strength of the interaction.

The binding to caveolin-1-1–101 could be reproduced in vitro with the use of a GST fusion protein and the recombinant histidine-tagged filamin fragment. In our in vitro binding assays, we observed that a C-terminally shortened filamin fragment was not able to bind to the GST–caveolin-1-1–101 fusion protein. Calculated from the mass difference between the 35- and 31-kDa fragments, the missing region should constitute about one-third of repeat 24 (35 amino acids). Thus, this deletion might destroy the conformation of repeat 24 and the neighboring hinge in a way that prevents caveolin-1 binding.

Unfortunately, the two-hybrid system could not be used to establish whether caveolin-1β interacted more strongly with filamin than caveolin-1α. Reporter genes were not activated, even when probing the well-known full-length caveolin-1–caveolin-1 interaction. This might be explained by a potential membrane association of full-length caveolin-1, a condition prohibiting the required translocation of two-hybrid complexes into the yeast nucleus. However, with another approach, the binding of full-length caveolin-1 to filamin could be confirmed. GST–full-length caveolin-1 fusion proteins bound to chicken muscle filamin in vitro. These binding experiments confirmed our initial findings with the two-hybrid system and indicated that caveolin-1 might be able to interact with the three filamin isoforms: nonmuscle filamin, muscle filamin, and β-filamin.

Confocal and electron microscopy showed that part of caveolin-1 and filamin was present in the same patches at the plasma membrane. In cells treated with CNF-1, intracellular caveolin-1–positive membranes apparently were reorganized and coaligned with filamin-decorated fibers. In cells with a few stress fibers, filamin immunoreactivity is partially observed between these actin bundles (Provance *et al.*, 1993). The fraction of filamin decorating stress fibers seems to increase upon Rho stimulation (this study). Therefore, we favor the explanation that the concomitant redistribution of caveolin-1–positive membrane domains to actin stress fibers is evoked by a caveolin-1–filamin interaction.

Our findings are similar to ultrastructural results by Senda *et al.* (1997) showing caveolae-like membrane domains adjacent to stress fibers in cells treated with *Bordetella bronchiseptica* dermonecrotic toxin (DNT). DNT, like CNF-1, activates Rho, a key regulator of the actin cytoskeleton (Fiorentini *et al.*, 1988; Horiguchi *et al.*, 1995). Interestingly, DNT also increases the amount of caveolae at the membrane facing the substratum (Senda *et al.*, 1997).

The dimensions of caveolae are smaller than the spatial resolution of the confocal microscope. Therefore, immunoelectron microscopy was applied to determine whether caveolae and filamin were tightly associated. In electron micrographs of trophoblasts stimulated with CNF-1, we found numerous small and large racemose clusters of caveolae, some of which were labeled for filamin. This supported our notion that actin filaments are connected to caveolar membranes via filamin.

We also noticed that there were few, if any, intracellular caveolin-1–positive vesicles in our electron microscopy specimens. This indicated that most of the apparently intracellular fluorescent signal for caveolin-1 might actually represent very deeply invaginated racemose caveolar clusters. Trophoblasts are flat and well-spread cells, and deep (a few hundred nanometers) invaginations would be difficult to distinguish from truly intracellular structures by confocal microscopy.

Together, the confocal and immunogold studies confirmed that caveolae and filamin could indeed associate in cells. Moreover, these data were perfectly compatible with a direct binding of caveolin-1 to filamin. At the same time, they showed that the extent of the detectable caveolae/caveolin-1–filamin interaction was limited. Considering our quantitative binding data from the two-hybrid experiments, it seems possible that caveolin-1β is the primary ligand for filamin. Western blotting revealed that trophoblasts, compared with NIH/3T3 fibroblasts, contained only minor amounts of caveolin-1β. This might account for the relatively sparse colocalization of filamin and caveolin-1.

Our findings fit well with previous reports describing relations of caveolae with the actin cytoskeleton. In an ear-

lier report (Izumi *et al.*, 1988), it was shown that the striped coat of caveolae could be decorated with myosin subfragment 1 and phalloidin, implying an association of actin with caveolae. In another study, the caveolar inositol 1,4,5-trisphosphate receptor–like protein was shown to coalign with actin filaments, and caveolae distribution was altered in response to treatment with CD (Fujimoto *et al.*, 1995). Biochemical evidence for the importance of the actin cytoskeleton in caveolar functions was provided in a report showing that the internalization of clustered caveolae, stimulated by okadaic acid, could be blocked by CD (Parton *et al.*, 1994). Furthermore, filamin is thought to play a role in cell locomotion and mechanoprotection, and it functions as a cytoskeletal linker for transmembrane proteins such as integrins and the glycoprotein I complex in platelets (Cunningham *et al.*, 1992; Meyer *et al.*, 1997; Glogauer *et al.*, 1998; Loo *et al.*, 1998; Pfaff *et al.*, 1998). Similarly, our results indicate that caveolin-1 is tethered to the cortical actin cytoskeleton via filamin.

It can only be speculated which function the caveolin-1–filamin interaction might have in cells. Filamin has been found to play a regulatory role in the endocytosis of the proprotein-processing proteinase furin. Filamin-deficient cells showed an increase in furin internalization and reduced furin sorting to the *trans*-Golgi network (Liu *et al.*, 1997). Although it is still not clear whether caveolae play any major role in clathrin-independent endocytosis (van Deurs *et al.*, 1993; Parton, 1996; Anderson, 1998), it is possible that filamin might also be involved in the regulation of caveolae internalization. This, in turn, could be important for signaling.

ACKNOWLEDGMENTS

We thank K. Pedersen, M. Ohlsen, U. Hjortenberg, and K. Ottosen for technical assistance, P. Boquet for kindly providing CNF-1, and C. Mitchelmore, L. Vogel, F. Vilhardt, and E.M. Danielsen for helpful discussions. This study was supported by grants to B.v.D. from the Human Frontier Science Program (RG404/96 M), the Danish Cancer Society, the Danish Medical Research Council, and the Novo Nordisk Foundation.

REFERENCES

Aktories, K. (1997). Rho proteins: targets for bacterial toxins. Trends Microbiol. *5*, 282–288.

Anderson, R.G. (1998). The caveolae membrane system. Annu. Rev. Biochem. *67*, 199–225.

Chang, W.J., Ying, Y.S., Rothberg, K.G., Hooper, N.M., Turner, A.J., Gambliel, H.A., De Gunzburg, J., Mumby, S.M., Gilman, A.G., and Anderson, R.G. (1994). Purification and characterization of smooth muscle cell caveolae. J. Cell Biol. *126*, 127–138.

Couet, J., Li, S., Okamoto, T., Ikezu, T., and Lisanti, M.P. (1997). Identification of peptide and protein ligands for the caveolin-scaffolding domain: implications for the interaction of caveolin with caveolae-associated proteins. J. Biol. Chem. *272*, 6525–6533.

Cunningham, C.C., Gorlin, J.B., Kwiatkowski, D.J., Hartwig, J.H., Janmey, P.A., Byers, H.R., and Stossel, T.P. (1992). Actin-binding protein requirement for cortical stability and efficient locomotion. Science *255*, 325–327.

Dupree, P., Parton, R.G., Raposo, G., Kurzchalia, T.V., and Simons, K. (1993). Caveolae and sorting in the trans-Golgi network of epithelial cells. EMBO J. *12*, 1597–1605.

Engelman, J.A., Wykoff, C.C., Yasuhara, S., Song, K.S., Okamoto, T., and Lisanti, M.P. (1997). Recombinant expression of caveolin-1 in oncogenically transformed cells abrogates anchorage-independent growth. J. Biol. Chem. *272*, 16374–16381.

Fiorentini, C., Arancia, G., Caprioli, A., Falbo, V., Ruggeri, F.M., and Donelli, G. (1988). Cytoskeletal changes induced in HEp-2 cells by the cytotoxic necrotizing factor of *Escherichia coli*. Toxicon *26*, 1047–1056.

Frangioni, J.V., and Neel, B.G. (1993). Solubilization and purification of enzymatically active glutathione S-transferase (pGEX) fusion proteins. Anal. Biochem. *210*, 179–187.

Fujimoto, T., Miyawaki, A., and Mikoshiba, K. (1995). Inositol 1,4,5-trisphosphate receptor-like protein in plasmalemmal caveolae is linked to actin filaments. J. Cell Sci. *108*, 7–15.

Garcia-Cardena, G., Fan, R., Stern, D.F., Liu, J., and Sessa, W.C. (1996). Endothelial nitric oxide synthase is regulated by tyrosine phosphorylation and interacts with caveolin-1. J. Biol. Chem. *271*, 27237–27240.

Gietz, R.D., and Schiestl, R.H. (1995). Transforming yeast with DNA. Methods Mol. Cell. Biol. *5*, 255–269.

Glenney, J.R., Jr. (1989). Tyrosine phosphorylation of a 22-kDa protein is correlated with transformation by Rous sarcoma virus. J. Biol. Chem. *264*, 20163–20166.

Glenney, J.R., Jr., and Soppet, D. (1992). Sequence and expression of caveolin, a protein component of caveolae plasma membrane domains phosphorylated on tyrosine in Rous sarcoma virus-transformed fibroblasts. Proc. Natl. Acad. Sci. USA *89*, 10517–10521.

Glogauer, M., Arora, P., Chou, D., Janmey, P.A., Downey, G.P., and McCulloch, C.A. (1998). The role of actin-binding protein 280 in integrin-dependent mechanoprotection. J. Biol. Chem. *273*, 1689–1698.

Gorlin, J.B., Yamin, R., Egan, S., Stewart, M., Stossel, T.P., Kwiatkowski, D.J., and Hartwig, J.H. (1990). Human endothelial actin-binding protein (ABP-280, nonmuscle filamin): a molecular leaf spring. J. Cell Biol. *111*, 1089–1105.

Horiguchi, Y., Senda, T., Sugimoto, N., Katahira, J., and Matsuda, M. (1995). *Bordetella bronchiseptica* dermonecrotizing toxin stimulates assembly of actin stress fibers and focal adhesions by modifying the small GTP-binding protein rho. J. Cell Sci. *108*, 3243–3251.

Izumi, T., Shibata, Y., and Yamamoto, T. (1988). Striped structures on the cytoplasmic surface membranes of the endothelial vesicles of the rat aorta revealed by quick-freeze, deep-etching replicas. Anat. Rec. *220*, 225–232.

Koleske, A.J., Baltimore, D., and Lisanti, M.P. (1995). Reduction of caveolin and caveolae in oncogenically transformed cells. Proc. Natl. Acad. Sci. USA *92*, 1381–1385.

Kurzchalia, T.V., Dupree, P., Parton, R.G., Kellner, R., Virta, H., Lehnert, M., and Simons, K. (1992). VIP21, a 21-kDa membrane protein is an integral component of trans-Golgi-network-derived transport vesicles. J. Cell Biol. *118*, 1003–1014.

Li, S., Couet, J., and Lisanti, M.P. (1996). Src tyrosine kinases, Gα subunits, and H-Ras share a common membrane-anchored scaffolding protein, caveolin: caveolin binding negatively regulates the auto-activation of Src tyrosine kinases. J. Biol. Chem. *271*, 29182–29190.

Li, S., Okamoto, T., Chun, M., Sargiacomo, M., Casanova, J.E., Hansen, S.H., Nishimoto, I., and Lisanti, M.P. (1995). Evidence for a regulated interaction between heterotrimeric G proteins and caveolin. J. Biol. Chem. *270*, 15693–15701.

Liu, G., Thomas, L., Warren, R.A., Enns, C.A., Cunningham, C.C., Hartwig, J.H., and Thomas, G. (1997). Cytoskeletal protein ABP-280 directs the intracellular trafficking of furin and modulates proprotein processing in the endocytic pathway. J. Cell Biol. *139*, 1719–1733.

Liu, J., Razani, B., Tang, S., Terman, B.I., Ware, J.A., and Lisanti, M.P. (1999). Angiogenesis activators and inhibitors differentially

regulate caveolin-1 expression and caveolae formation in vascular endothelial cells: angiogenesis inhibitors block vascular endothelial growth factor-induced down-regulation of caveolin-1. J. Biol. Chem. *274*, 15781–15785.

Loo, D.T., Kanner, S.B., and Aruffo, A. (1998). Filamin binds to the cytoplasmic domain of the β1-integrin: identification of amino acids responsible for this interaction. J. Biol. Chem. *273*, 23304–23312.

Meyer, S.C., Zuerbig, S., Cunningham, C.C., Hartwig, J.H., Bissell, T., Gardner, K., and Fox, J. (1997). Identification of the region in actin-binding protein that binds to the cytoplasmic domain of glycoprotein IBα. J. Biol. Chem. *272*, 2914–2919.

Monier, S., Parton, R.G., Vogel, F., Behlke, J., Henske, A., and Kurzchalia, T.V. (1995). VIP21-caveolin, a membrane protein constituent of the caveolar coat, oligomerizes in vivo and in vitro. Mol. Biol. Cell *6*, 911–927.

Mukherjee, S., Zha, X., Tabas, I., and Maxfield, F.R. (1998). Cholesterol distribution in living cells: fluorescence imaging using dehydroergosterol as a fluorescent cholesterol analog. Biophys. J. *75*, 1915–1925.

Oh, P., and Schnitzer, J.E. (1999). Immunoisolation of caveolae with high affinity antibody binding to the oligomeric caveolin cage: toward understanding the basis of purification. J. Biol. Chem. *274*, 23144–23154.

Oka, N., Yamamoto, M., Schwencke, C., Kawabe, J., Ebina, T., Ohno, S., Couet, J., Lisanti, M.P., and Ishikawa, Y. (1997). Caveolin interaction with protein kinase C: isoenzyme-dependent regulation of kinase activity by the caveolin scaffolding domain peptide. J. Biol. Chem. *272*, 33416–33421.

Okamoto, T., Schlegel, A., Scherer, P.E., and Lisanti, M.P. (1998). Caveolins, a family of scaffolding proteins for organizing "preassembled signaling complexes" at the plasma membrane. J. Biol. Chem. *273*, 5419–5422.

Parton, R.G. (1996). Caveolae and caveolins. Curr. Opin. Cell Biol. *8*, 542–548.

Parton, R.G., Joggerst, B., and Simons, K. (1994). Regulated internalization of caveolae. J. Cell Biol. *127*, 1199–1215.

Petersen, O.W., Hansen, S.H., Laursen, I., and van Deurs, B. (1989). Effect of insulin on growth and expression of smooth muscle isoactin in human breast gland myoepithelial cells in a chemically defined culture system. Eur. J. Cell Biol. *50*, 500–509.

Pfaff, M., Liu, S., Erle, D.J., and Ginsberg, M.H. (1998). Integrin beta cytoplasmic domains differentially bind to cytoskeletal proteins. J. Biol. Chem. *273*, 6104–6109.

Provance, D.W., Jr., McDowall, A., Marko, M., and Luby-Phelps, K. (1993). Cytoarchitecture of size-excluding compartments in living cells. J. Cell Sci. *106*, 565–577.

Ridley, A.J., and Hall, A. (1992). The small GTP-binding protein rho regulates the assembly of focal adhesions and actin stress fibers in response to growth factors. Cell *70*, 389–399.

Rohlich, P., and Allison, A.C. (1976). Oriented pattern of membrane-associated vesicles in fibroblasts. J. Ultrastruct Res. *57*, 94–103.

Rothberg, K.G., Heuser, J.E., Donzell, W.C., Ying, Y.S., Glenney, J.R., and Anderson, R.G. (1992). Caveolin, a protein component of caveolae membrane coats. Cell *68*, 673–682.

Sargiacomo, M., Scherer, P.E., Tang, Z., Kubler, E., Song, K.S., Sanders, M.C., and Lisanti, M.P. (1995). Oligomeric structure of caveolin: implications for caveolae membrane organization. Proc. Natl. Acad. Sci. USA *92*, 9407–9411.

Sargiacomo, M., Sudol, M., Tang, Z., and Lisanti, M.P. (1993). Signal transducing molecules and glycosyl-phosphatidylinositol-linked proteins form a caveolin-rich insoluble complex in MDCK cells. J. Cell Biol. *122*, 789–807.

Scheiffele, P., Verkade, P., Fra, A.M., Virta, H., Simons, K., and Ikonen, E. (1998). Caveolin-1 and -2 in the exocytic pathway of MDCK cells. J. Cell Biol. *140*, 795–806.

Scherer, P.E., Lewis, R.Y., Volonte, D., Engelman, J.A., Galbiati, F., Couet, J., Kohtz, D.S., van Donselaar, E., Peters, P., and Lisanti, M.P. (1997). Cell-type and tissue-specific expression of caveolin-2: caveolins 1 and 2 colocalize and form a stable hetero-oligomeric complex in vivo. J. Biol. Chem. *272*, 29337–29346.

Scherer, P.E., Okamoto, T., Chun, M., Nishimoto, I., Lodish, H.F., and Lisanti, M.P. (1996). Identification, sequence, and expression of caveolin-2 defines a caveolin gene family. Proc. Natl. Acad. Sci. USA *93*, 131–135.

Scherer, P.E., Tang, Z., Chun, M., Sargiacomo, M., Lodish, H.F., and Lisanti, M.P. (1995). Caveolin isoforms differ in their N-terminal protein sequence and subcellular distribution: identification and epitope mapping of an isoform-specific monoclonal antibody probe. J. Biol. Chem. *270*, 16395–16401.

Schnitzer, J.E., Oh, P., Jacobson, B.S., and Dvorak, A.M. (1995). Caveolae from luminal plasmalemma of rat lung endothelium: microdomains enriched in caveolin, Ca(2+)-ATPase, and inositol trisphosphate receptor. Proc. Natl. Acad. Sci. USA *92*, 1759–1763.

Schroeder, F., Jefferson, J.R., Kier, A.B., Knittel, J., Scallen, T.J., Wood, W.G., and Hapala, I. (1991). Membrane cholesterol dynamics: cholesterol domains and kinetic pools. Proc. Soc. Exp. Biol. Med. *196*, 235–252.

Senda, T., Horiguchi, Y., Umemoto, M., Sugimoto, N., and Matsuda, M. (1997). *Bordetella bronchiseptica* dermonecrotizing toxin, which activates a small GTP-binding protein rho, induces membrane organelle proliferation and caveolae formation. Exp. Cell Res. *230*, 163–168.

Slot, J.W., Geuze, H.J., Gigengack, S., Lienhard, G.E., and James, D.E. (1991). Immuno-localization of the insulin regulatable glucose transporter in brown adipose tissue of the rat. J. Cell Biol. *113*, 123–135.

Smart, E.J., Ying, Y.S., Conrad, P.A., and Anderson, R.G. (1994). Caveolin moves from caveolae to the Golgi apparatus in response to cholesterol oxidation. J. Cell Biol. *127*, 1185–1197.

Smart, E.J., Ying, Y.S., Mineo, C., and Anderson, R.G. (1995). A detergent-free method for purifying caveolae membrane from tissue culture cells. Proc. Natl. Acad. Sci. USA *92*, 10104–10108.

Stan, R.V., Roberts, W.G., Predescu, D., Ihida, K., Saucan, L., Ghitescu, L., and Palade, G.E. (1997). Immunoisolation and partial characterization of endothelial plasmalemmal vesicles (caveolae). Mol. Biol. Cell *8*, 595–605.

Takafuta, T., Wu, G., Murphy, G.F., and Shapiro, S.S. (1998). Human β-filamin is a new protein that interacts with the cytoplasmic tail of glycoprotein Ibα. J. Biol. Chem. *273*, 17531–17538.

van Deurs, B., Holm, P.K., Sandvig, K., and Hansen, S.H. (1993). Are caveolae involved in clathrin-independent endocytosis? Trends Cell Biol. *3*, 249–251.

van Deurs, B., Nilausen, K., Faergeman, O., and Meinertz, H. (1982). Coated pits and pinocytosis of cationized ferritin in human skin fibroblasts. Eur. J. Cell Biol. *27*, 270–278.

Vogel, U., Sandvig, K., and van Deurs, B. (1998). Expression of caveolin-1 and polarized formation of invaginated caveolae in Caco-2 and MDCK II cells. J. Cell Sci. *111*, 825–832.